

Magnetic anisotropy in MnGe thin films and its evolution under external magnetic fields

Zhaohang Li(李朝航), Fanbao Meng(孟凡保), Kesen Zhao(赵科森), Tao Qi(齐涛), Shihao Liu(刘仕豪), Zongyao Huang(黄宗耀), Feixiong Quan(全飞熊), Zhiwei Wang(王智炜), Zhengjie Wang(王郑杰), Xigang Luo(罗习刚), Jianjun Ying(应剑俊), Yubin Hou(侯玉斌), Wenjie Meng(孟文杰), Qingyou Lu(陆轻铀), and Xianhui Chen(陈仙辉)

Citation: Chin. Phys. B, 2026, 35 (**1**): 016802. DOI: 10.1088/1674-1056/ae1191
http://cpb.iphy.ac.cn; http://iopscience.iop.org/cpb

What follows is a list of articles you may be interested in

Molecular beam epitaxial growth and physical properties of AlN/GaN superlattices with an average 50% Al composition

Siqi Li(李思琦), Pengfei Shao(邵鹏飞), Xiao Liang(梁潇), Songlin Chen(陈松林), Zhenhua Li(李振华), Xujun Su(苏旭军), Tao Tao(陶涛), Zili Xie(谢自力), Bin Liu(刘斌), M. Ajmal Khan, Li Wang, T. T. Lin, Hideki Hirayama, Rong Zhang(张荣), and Ke Wang(王科)

Chin. Phys. B, 2024, 33 (**12**): 126801. DOI: 10.1088/1674-1056/ad84cc

Atomically self-healing of structural defects in monolayer WSe_2

Kangshu Li(李康舒), Junxian Li(李俊贤), Xiaocang Han(韩小藏), Wu Zhou(周武), and Xiaoxu Zhao(赵晓续)

Chin. Phys. B, 2024, 33 (**9**): 096804. DOI: 10.1088/1674-1056/ad641f

Bimodal growth of Fe islands on graphene

Yi-Sheng Gu(顾翊晟), Qiao-Yan Yu(俞俏滟), Dang Liu(刘荡), Ji-Ce Sun(孙蓟策), Rui-Jun Xi(席瑞骏), Xing-Sen Chen(陈星森), Sha-Sha Xue(薛莎莎), Yi Zhang(章毅), Xian Du(杜宪), Xu-Hui Ning(宁旭辉), Hao Yang(杨浩), Dan-Dan Guan(管丹丹), Xiao-Xue Liu(刘晓雪), Liang Liu(刘亮), Yao-Yi Li(李耀义), Shi-Yong Wang(王世勇), Can-Hua Liu(刘灿华), Hao Zheng(郑浩), and Jin-Feng Jia(贾金锋)

Chin. Phys. B, 2024, 33 (**6**): 068104. DOI: 10.1088/1674-1056/ad322f

Microscopic growth mechanism and edge states of monolayer 1T'-$MoTe_2$

Haipeng Zhao(赵海鹏), Yin Liu(刘隐), Shengguo Yang(杨胜国), Chenfang Lin(林陈昉), Mingxing Chen(陈明星), Kai Braun, Xinyi Luo(罗心仪), Siyu Li(李思宇), Anlian Pan(潘安练), and Xiao Wang(王笑)

Chin. Phys. B, 2024, 33 (**4**): 046801. DOI: 10.1088/1674-1056/ad16d5

Growth and characterization of Bi(110)/$CrTe_2$ heterostructures: Exploring interplay between magnetism and topology

Zhenyu Yuan(袁震宇), Fazhi Yang(杨发枝), Baiqing Lv(吕佰晴), Yaobo Huang(黄耀波), Tian Qian(钱天), Jinpeng Xu(徐金朋), and Hong Ding(丁洪)

Chin. Phys. B, 2024, 33 (**2**): 026802. DOI: 10.1088/1674-1056/ad082a

---

RAPID COMMUNICATION

Magnetic anisotropy in MnGe thin films and its evolution under external magnetic fields

Zhaohang Li(李朝航)[1,†], Fanbao Meng(孟凡保)[1,†], Kesen Zhao(赵科森)[1,2], Tao Qi(齐涛)[1], Shihao Liu(刘仕豪)[1], Zongyao Huang(黄宗耀)[1], Feixiong Quan(全飞熊)[1], Zhiwei Wang(王智炜)[1], Zhengjie Wang(王郑杰)[1], Xigang Luo(罗习刚)[1], Jianjun Ying(应剑俊)[1], Yubin Hou(侯玉斌)[2], Wenjie Meng(孟文杰)[2], Qingyou Lu(陆轻铀)[1,2], and Xianhui Chen(陈仙辉)[1,3,4,‡]

[1] *Department of Physics, University of Science and Technology of China, Hefei* 230026, *China*
[2] *Anhui Key Laboratory of Low-Energy Quantum Materials and Devices, High Magnetic Field Laboratory, Hefei Institutes of Physical Science, Chinese Academy of Sciences, Hefei* 230026, *China*
[3] *CAS Center for Excellence in Superconducting Electronics (CENSE), Shanghai* 200050, *China*
[4] *CAS Center for Excellence in Quantum Information and Quantum Physics, Hefei* 230026, *China*

(Received 1 September 2025; revised manuscript received 9 October 2025; accepted manuscript online 10 October 2025)

Chiral magnets have attracted considerable attention due to their intricate magnetic properties, among which B20 compounds constitute a quintessential class that has gained significant focus, particularly in the study of skyrmions. MnGe, as a member of the B20 family, exhibits a more complex magnetic structure compared with other materials with similar crystal structures. In this work, we successfully synthesized high-quality MnGe thin films and characterized their magnetoresistance, *M*–*H* curves, magneto-Seebeck effect, and magnetic force microscopy (MFM) images, all of which demonstrate pronounced magnetic anisotropy. Notably, the Seebeck coefficient exhibits a plateau at low magnetic fields when the magnetic field is applied in the film plane, indicating a field region in which the magnetic structure remains stable. MFM imaging further reveals magnetic transitions within the MnGe films when the magnetic field is oriented along the film plane. These findings are crucial for advancing our understanding of the magnetic ground state of MnGe and the evolution of its magnetic structure under an applied external magnetic field.

Keywords: molecular beam epitaxy, chiral magnets, thin film, magnetic anisotropy, magnetic force microscopy

PACS: 68.37.Rt, 68.55.–a, 73.61.–r, 73.63.–b

DOI: 10.1088/1674-1056/ae1191 **CSTR:** 32038.14.CPB.ae1191

1. Introduction

In recent decades, B20 materials have emerged as a pivotal platform for hosting magnetic skyrmions, owing to their unique noncentrosymmetric crystal symmetry that enables the Dzyaloshinskii–Moriya interaction (DMI).[1–8] Magnetic B20 materials, such as MnSi, typically exhibit a helical magnetic structure and display a skyrmion phase within specific magnetic field–temperature ranges.[1–3] In contrast, MnGe possesses a more intricate magnetic structure, comprising three mutually orthogonal helical axes, resulting in a unique hedgehog lattice arrangement.[9–12] This complexity endows MnGe with a broader range of physical properties compared with other B20 materials, including an extended skyrmion phase across a larger magnetic field–temperature range,[9] a more pronounced topological Hall effect,[10] substantial anomalous Hall conductance at high fields,[11] and the potential for momentum-space topological properties.[13]

The magnetic structure of MnGe thin films differs significantly from that of bulk samples. In MnGe films, the helical axes, which are aligned along the [001], [100], and [010] directions in the crystal, tilt toward the [111] direction, with the tilt angle depending on the film thickness. As the film thickness decreases, the three helical axes converge, and a triple-*q* state in the MnGe film transforms into a single-*q* state when a magnetic field is applied along the [111] direction or the temperature is increased.[10] In summary, the application of a magnetic field or an increase in temperature ultimately leads to the merging of the three helical axes into a single axis along the [111] direction, in contrast to bulk samples, which are able to sustain a triple-*q* state even under high magnetic fields.[12] Direct observations using spin-polarized scanning tunneling microscopy (SP-STM) have shown that the magnetic ground state of MnGe films consists of multiple domains, each with a single helical axis,[14] which contradicts the previously reported triple-*q* state of MnGe thin films. One possible explanation for this discrepancy is sample dependence,[15] which highlights the sensitivity of the magnetic ground state to external factors such as growth methods and film thickness. Conse-

[†]These authors contributed equally to this work.
[‡]Corresponding author. E-mail: chenxh@ustc.edu.cn
© 2026 Chinese Physical Society and IOP Publishing Ltd. All rights, including for text and data mining, AI training, and similar technologies, are reserved.

quently, the magnetic structure of MnGe is not only inherently complex but also highly susceptible to variations under different conditions (e.g., thickness, temperature, and magnetic field). Therefore, it is crucial to investigate the evolution of the magnetic structure of MnGe thin films in response to changes in magnetic field and temperature, employing both experimental and theoretical approaches, although to date there has been no systematic study addressing the variations in the magnetic structure of MnGe thin films.

In this study, we investigated the magnetotransport and magnetic properties of MnGe thin films under two distinct orientations of the magnetic field: parallel to the film plane ($H\|[111]$) and perpendicular to the film plane ($H\perp[111]$). It was observed that MnGe films exhibit pronounced magnetic anisotropy. Additionally, multiple phase transitions were identified when the magnetic field was applied along the direction perpendicular to [111], which were also reflected in the magnetoresistance, M–H data, magnetic force microscope (MFM) images, and Seebeck coefficients. By systematically analyzing the experimental results, we constructed a phase diagram for the magnetic field perpendicular to [111] orientation. This phase diagram provides a clearer understanding of the magnetic structure evolution in MnGe thin films, offering valuable insights that will aid in the future exploration of the material's physical properties.

2. Experimental details

2.1. Thin-film growth

The MnGe thin films were grown via molecular beam epitaxy (MBE),[16] and to minimize substrate thermal conductivity effects during Seebeck measurements, a 0.1-mm-thick Si substrate was employed. The Si (111) substrate was first immersed in an HF acid buffer for 2 hours and then transferred to a vacuum chamber with a base pressure of 5×10^{-10} mbar. Prior to growth, the substrate was annealed at 800 °C for 8 hours to achieve a 7×7 superlattice structure. Subsequently, a 2-nm-thick MnSi buffer layer was deposited onto the Si substrate by evaporating Mn at 400 °C. Following this, Mn and Ge were co-evaporated at 90 °C onto the buffer layer in a Mn:Ge ratio of $1:\sim1$. Finally, the film was annealed at 300 °C for 2 hours.

2.2. Characterization and measurements

The quality of the samples was characterized by x-ray diffraction (XRD) using Cu $K\alpha$ radiation (SmartLab-9, Rigaku Corp.). The temperature and magnetic field dependence of the magnetic and thermal transport properties were measured using a standard four-probe configuration in the physical properties measurement system (Quantum Design PPMS-9 T). In the thermal transport experiments, the sample was mounted on a custom-built thermoelectric puck, and measurements were conducted under high-vacuum conditions (with a pressure lower than 1×10^{-5} Torr). The lowest temperature reached during the measurements was 30 K, and the magnetic field sweep rate was set to 3 mT/s. The magnetic properties of the samples were evaluated using a vibrating sample magnetometer (Quantum Design VSM-7 T). Additionally, the magnetic domain distribution on the sample surface was investigated using a home-built cryogenic rotating MFM system (12 T), employing commercial piezoresistive cantilevers (Quantum Design Co., Ltd., model PRSA-L400-F30-Si-sdPCB) with a resonance frequency of approximately 35 kHz and a quality factor of about 10000 at 5 K.

3. Results and discussion

3.1. Characterization of the MnGe films

Figure 1 shows the characterization of the MnGe films. Figure 1(a) shows the crystal structure of MnGe, and Fig. 1(b) presents the XRD data of the films. All film thicknesses used in this article are 20 nm, and the 2 μm × 2 μm atomic force microscopy (AFM) image shown in Fig. 1(c) reveals a relatively flat surface, indicating the high quality of the film. To further substantiate the quality of our films, we have provided a direct comparison between the AFM image of our sample (Fig. 1(c)) and those reported in the literature.[14,16] The AFM image of our film reveals an exceptionally flat surface topography with only a low density of pores. This stands in sharp contrast to literature reports on MnGe films, which frequently describe poor film continuity, manifested as either a high density of bright protrusions[14] or a distinct island-growth mode.[16] The observed morphological differences provide strong evidence for the superior quality of our samples. Additionally, the reflection high-energy electron diffraction (RHEED) pattern of the MnGe film, featuring sharp streaks, suggests well-defined two-dimensional film growth, as depicted in Fig. 1(d), which is consistent with previous reports.[16]

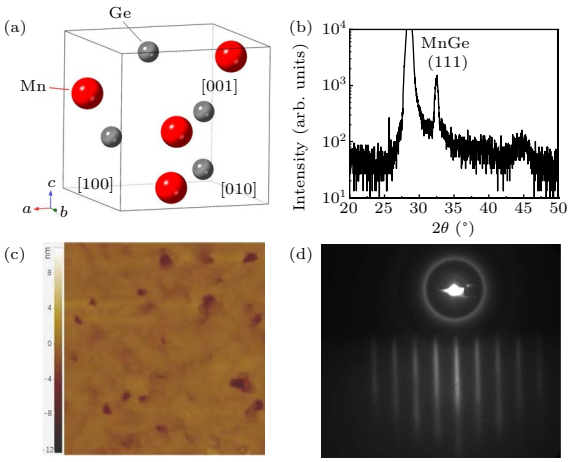


Fig. 1. (a) The crystal structure of MnGe. (b) XRD patterns of the MnGe thin film. (c) 2 μm × 2 μm AFM image of the MnGe thin film. (d) RHEED pattern of the MnGe thin film, indicating the high quality of the sample.

3.2. Magnetic and transport properties measurements of MnGe thin films

Figures 2(a) and 2(b) show the magnetic-field dependence of the magnetoresistance at various temperatures when the magnetic field is applied along the current direction (within the film plane) and perpendicular to the (111) plane (out of the film plane). The up-sweep and down-sweep curves exhibit clear hysteresis, indicating the formation of magnetic ordering. As shown in Fig. 2(a), at low temperatures ($T = 2$ K) with H parallel to the film plane, the magnetoresistance shows positive values under low magnetic fields and negative values under high magnetic fields. As the temperature increases, the positive magnetoresistance features gradually weaken and eventually disappear for $T > 150$ K, with the magnetoresistance becoming entirely negative. In contrast, when the magnetic field is applied perpendicular to the (111) plane, as shown in Fig. 2(b), the magnetoresistance exhibits negative values throughout the entire temperature range, which is markedly different from the behavior observed when the magnetic field is aligned with the current direction in Fig. 2(a).

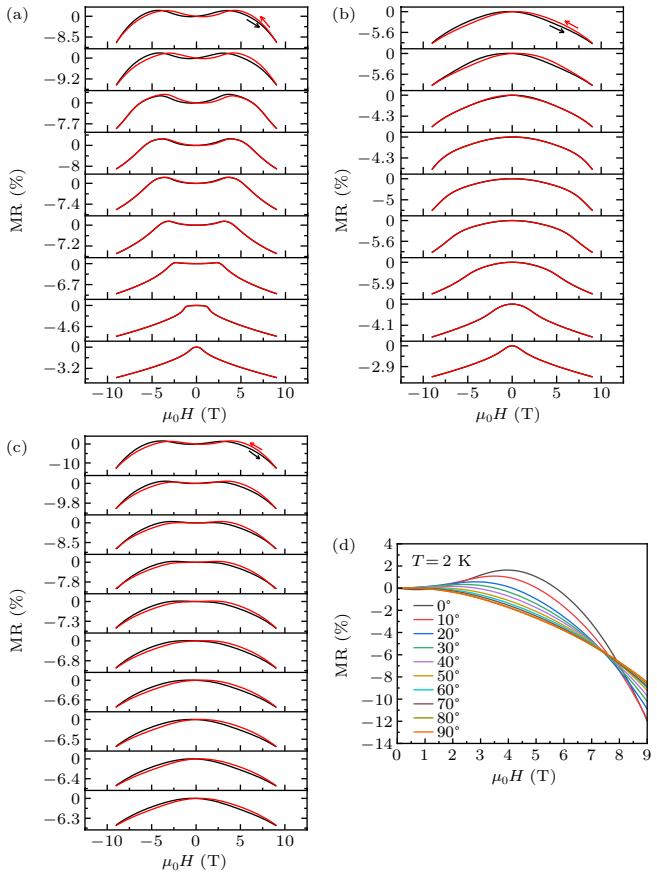


Fig. 2. (a)–(b) Magnetoresistance data at different temperatures with (a) $H\|$ film plane and (b) $H\perp$ film plane. The up-sweep and down-sweep curves do not overlap at the same temperature, indicating a hysteresis phenomenon. (c)–(d) Magnetoresistance data at $T = 2$ K with the magnetic field rotating in the out-of-plane direction from 0° ($H\|$ film plane) to 90° ($H\perp$ film plane).

It is noteworthy that the magnetoresistance behavior observed for H parallel to the (111) plane is similar to that seen in polycrystalline MnGe, where the magnetoresistance response transitions from positive in the low-field regime to negative in the high-field regime.[17,18] The positive magnetoresistance observed here is unconventional, as an external magnetic field typically suppresses spin-dependent scattering, leading to monotonically increasing negative magnetoresistance in other related B20-type compounds. The large positive magnetoresistance observed in polycrystalline MnGe samples is attributed to fluctuations of the emergent magnetic field (monopole fluctuations), and the significant positive magnetoresistance, peaking around the magnetic phase boundary, is ascribed to the enhancement of monopole fluctuations near the monopole–antimonopole annihilation point. To further investigate the magnetoresistance changes for H parallel and H perpendicular to the (111) plane in thin films, we measured the magnetoresistance at $T = 2$ K with the magnetic field rotating in the out-of-plane direction, from 0° ($H\|$ film plane) to 90° ($H\perp$ (111) plane). Figure 2(c) presents magnetoresistance data measured at different rotation angles. Figure 2(d) compiles the magnetoresistance data from all angles, facilitating a clearer analysis of the trend in magnetoresistance variation with angle. A clear transition to entirely negative magnetoresistance behavior occurs around a rotation angle of approximately 40° (starting from 0°), indicating that monopole fluctuations are unlikely to be the origin of the positive magnetoresistance behavior in the film. Compared with the behavior under a magnetic field perpendicular to the (111) plane, the parallel alignment of the magnetic field with the (111) plane may induce an additional magnetic phase transition.

The anisotropic magnetic-field responses are further evidenced by the sharp contrasts observed in other physical properties for H parallel and H perpendicular to the (111) plane configurations. Figure 3 illustrates the H dependence of M for both H parallel and H perpendicular to the plane. At 300 K, both configurations exhibit a linear H dependence of M, but as the temperature decreases to 200 K, nonlinear behavior with saturation of M at high magnetic fields becomes evident. Below 200 K, the behaviors diverge significantly: an obvious metamagnetic transition is observed for H parallel to the (111) plane, with the transition point shifting to higher fields as the temperature decreases. For clarity of analysis, the transition point in the M–H curve of Fig. 3(a) is defined as H_k. This behavior aligns with the magnetoresistance data presented in Fig. 2(a), where positive magnetoresistance under H parallel to the (111) plane at low fields begins to appear as the temperature is reduced to $T \leq 150$ K. In marked contrast, when the magnetic field is applied perpendicular to the (111) plane (as shown in Fig. 3(b)), the M–H curve exhibits an overall linear behavior below 200 K, which is consistent with the negative magnetoresistance observed in Fig. 2(b). Crucially, when the magnetic field is applied perpendicular to the (111)

plane, the M–H curves do not exhibit a transition point, unlike the behavior observed under in-plane field configurations. The distinct differences in behavior between the two magnetic field orientations indicate the presence of significant magnetic anisotropy.

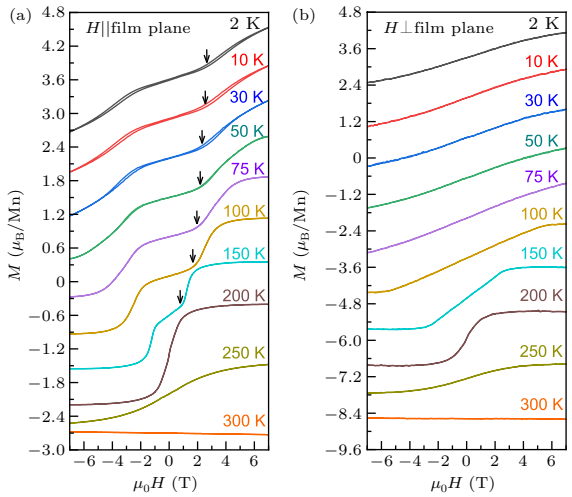


Fig. 3. The M–H curves of the MnGe thin film at different temperatures with (a) $H\|$ film plane and (b) $H\perp$ film plane. To facilitate subsequent analysis, the transition point in Fig. 3(a) is defined as H_k, as indicated by the black arrow.

Figures 4(a) and 4(b) display the magneto-Seebeck effect in MnGe films under magnetic fields applied along different directions. Figure 4(a) shows the variation of the Seebeck coefficient with magnetic field at different temperatures when H is parallel to the (111) plane. At low magnetic fields, the S–T curve exhibits a plateau, with no significant change in the Seebeck coefficient under the application of an in-plane magnetic field. As the magnetic field increases, a marked increase in the Seebeck coefficient is observed, followed by saturation at high magnetic fields. In other words, within a certain low magnetic-field range, the Seebeck coefficient remains unchanged and then increases abruptly beyond a specific field (defined as H_s). Moreover, this magnetic field corresponds exactly to H_k defined in Fig. 3(a). As the temperature increases, the magnetic-field range of the plateau gradually narrows and completely disappears at $T = 200$ K, which is consistent with the magnetic transition temperature of the MnGe thin film, indicating that the variation in the Seebeck effect of the MnGe thin film is closely related to changes in its magnetic properties. In contrast, when H is applied perpendicular to the (111) plane, as shown in Fig. 4(b), the S–T curve exhibits a parabolic behavior. Additionally, a ferromagnetic kink appears, similar to that observed in the S–T curve under H parallel to the (111) plane. Figures 4(c) and 4(d) show Seebeck–temperature curves at different magnetic fields with H parallel and perpendicular to the (111) plane, respectively. As shown in Fig. 4(c), when the magnetic field is applied parallel to the (111) plane, the curves at lower magnetic fields (e.g., 0 T, 1 T, and 2 T) coincide below specific temperatures (such as 100 K and below). This overlap behavior is consistent with the plateau observed in the low-field Seebeck data in Fig. 4(a). In contrast, when the field is oriented perpendicular to the (111) plane, the S–T curves exhibit negligible overlap across different magnetic fields, a feature consistent with the Seebeck data presented in Fig. 4(b). The Seebeck coefficient of MnGe is primarily related to changes in the magnetic structure, as observed in polycrystalline samples.[18] This suggests that at low magnetic fields with H parallel to the (111) plane, the magnetic structure of the MnGe film remains unchanged, whereas no similar plateau region is observed when H is perpendicular to the (111) plane, consistent with the M–H curve data (i.e., nonlinear behavior for H parallel to the (111) plane and linear behavior for H perpendicular to the (111) plane). In other words, when the magnetic field is applied parallel to the (111) plane, the magnetic structure remains stable at low fields. Given that the variation of the Seebeck coefficient directly correlates with changes in the magnetic structure, the Seebeck coefficient consequently exhibits minimal variation under low-field conditions, manifesting as the plateau behavior observed in Fig. 4(a). Conversely, with an out-of-plane magnetic field (perpendicular to the (111) plane), the magnetic structure undergoes continuous modification, resulting in a monotonic increase in the Seebeck coefficient with increasing magnetic field. Thus, these observations provide clear experimental evidence supporting the conclusion that the Seebeck coefficient in MnGe depends on changes in the magnetic structure.

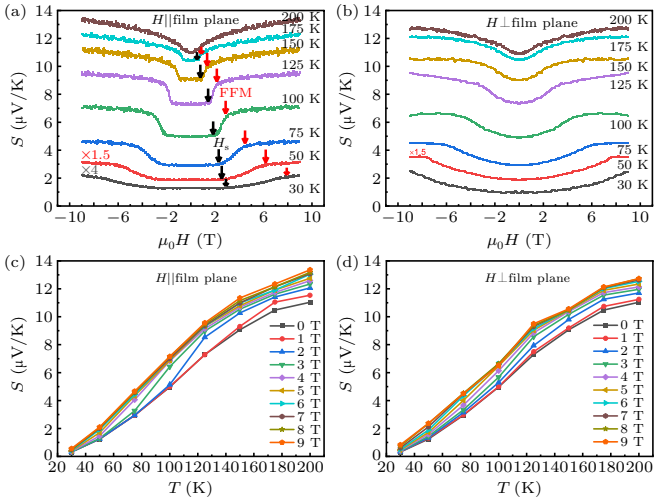


Fig. 4. (a)–(b) The magneto-Seebeck effect of the MnGe thin film at different temperatures with (a) $H\|$ film plane and (b) $H\perp$ film plane. The termination point of the magnetic-field plateau is defined as H_s, with both H_s and the forced-ferromagnetic (FFM) transition point indicated by black and red arrows, respectively. (c)–(d) Seebeck–temperature curves at different magnetic fields with (c) $H\|$ film plane and (d) $H\perp$ film plane.

4. Magnetic phase diagram of MnGe thin films

Based on the magnetoresistance, M–H curves, and Seebeck coefficient data, we constructed a phase diagram for H

parallel to the (111) plane, as shown in Fig. 5. The magnetic ground state used in this phase diagram was the multi-domain helical state, as confirmed by SP-STM.[14] To delineate the boundaries of the phase transition, we integrated data from the magnetoresistance, *M*–*H* curves, and Seebeck coefficient, as presented in Fig. 5. Detailed information on how data points were selected from each curve can be found in the supplementary materials (Fig. S1). Here, FFM (*M*–*H*) and FFM (Seebeck) are the forced-ferromagnetic transition points defined by the inflection points in the *M*–*H* curves and Seebeck data, respectively. It is evident that at low magnetic fields, the magnetic structure remains unchanged. As the magnetic field increases, the magnetic structure begins to evolve, which is marked as the transition region, and ultimately, the system enters a ferromagnetic state at higher magnetic fields. The maximum magnetoresistance value resides within the transition region. One possible explanation for this observation is that the phase transition from a multi-domain state to a single-domain state occurs when the magnetoresistance reaches its maximum value, in which scenario the magnetoresistance behaves as positive in the multi-domain state and negative in the single-domain state. Consequently, employing complementary experimental techniques to probe the magnetic evolution within the transition region is essential.

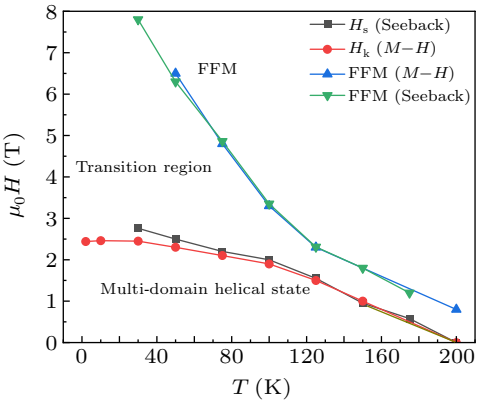


Fig. 5. The phase diagram with $H\|$ film plane, based on the magnetoresistance, *M*–*H* curves, and Seebeck coefficient data. Here, H_s and H_k correspond to the termination points of the magnetic-field plateau in the Seebeck data and the transition point in the *M*–*H* curves, respectively. Meanwhile, FFM (*M*–*H*) and FFM (Seebeck) denote FFM transition points defined by the inflection points in the corresponding *M*–*H* curves and Seebeck data.

For elucidating magnetic phase transitions within the transition region, microscopic magnetic characterization serves as a uniquely direct and effective experimental probe. To date, there is no direct microscopic experimental evidence confirming whether the magnetic structure remains unchanged at low magnetic fields. Commonly used methods for observing magnetic domain structures include Lorentz transmission electron microscopy,[19,20] SP-STM,[21,22] and MFM.[23,24] The following presents our observations of the magnetic domain structure using a custom-built rotatable low-temperature high-field MFM.[25,26] It is important to note that this device allows direct rotation of the microscope within a 12 T superconducting magnet inside a 5 K chamber, enabling us to capture high-resolution magnetic domain images (with a resolution better than 50 nm) under in-plane magnetic fields up to 12 T, which is critical for our study. The frequency-modulated mode is employed to image the stray field from the sample, with the frequency shift being proportional to the gradient of the magnetic interaction force at the cantilever tip. By maintaining a constant distance between the tip and the sample, the detected frequency shift can be used to infer the magnetic moment strength of the sample. We present MFM images at $T = 100$ K under varying magnetic fields when H is parallel to the (111) plane. We were unable to observe the three fundamental classes of domain walls and helical domains, which are typically found in FeGe, in our MFM images,[27–29] likely due to the much smaller helical period of MnGe (~ 3 nm), which is below the resolution limit of our MFM (~ 50 nm). As a result, we cannot directly observe changes in the MFM images with varying magnetic fields to determine the specific modifications in the magnetic domains. Even so, to reflect the rate of change in the magnetic signal as the magnetic field increases, we subtract the MFM images of each adjacent magnetic field. The calculation formula is as follows:

$$\Delta\text{phase}(H_1, H_2) = \frac{\text{phase}(H_2) - \text{phase}(H_1)}{H_2 - H_1}. \tag{1}$$

The contrast (phase degree) is proportional to the second derivative of the magnetic field, and the phase value represents the strength of the magnetic signal. Figure 6 shows the rate of change at $T = 100$ K, while the original data at $T = 100$ K are presented in Fig. S2 of the supplementary material. It can be observed that when $H < 2$ T, the magnetic signal remains unchanged, corresponding to the multi-domain helical state shown in Fig. 5. When $2\text{ T} < H < 3$ T, the magnetic structure changes most rapidly, corresponding to the transition region in Fig. 5, and as the magnetic field continues to increase, the system enters the ferromagnetic state, and the intensity of the magnetic signal stabilizes, as shown in Fig. 6(j). The quantitative analysis of the MFM data at 100 K is presented in Fig. S3, and by establishing a one-to-one correspondence between different phases of the phase diagram and the MFM images, we can confirm the accuracy of the phase diagram. This also aids in better understanding the changes in the magnetic structure, although we still cannot conclusively determine whether other magnetic phase transitions exist within the transition region, which may require more precise measurements in future experiments.

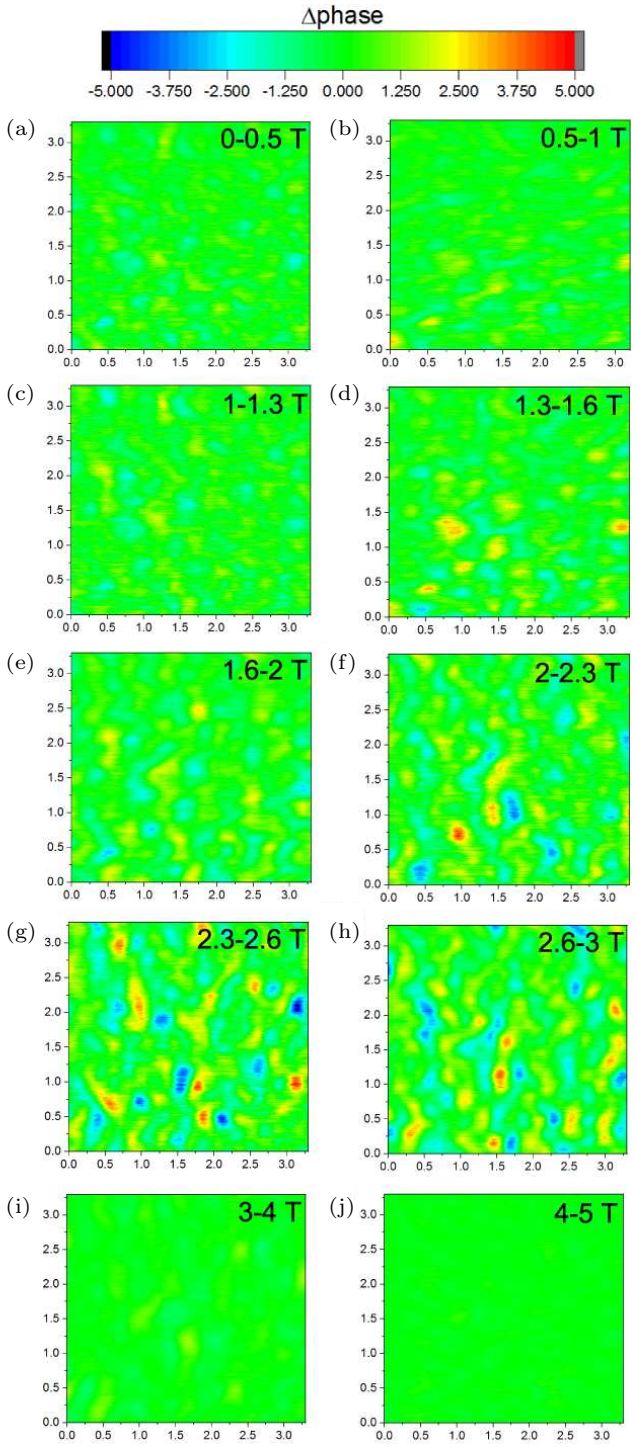


Fig. 6. The rate of change of the 3.3 μm × 3.3 μm MFM images at $T = 100$ K. In each figure, H_1–H_2 represents $\Delta\text{phase}(H_1, H_2)$.

5. Conclusion and perspectives

To understand the physical origin of the magnetic anisotropy in MnGe films, we compared the magnetoresistance and M–H behavior with those observed in FeGe and MnSi films,[30,31] whose magnetic ground states are also helical but with the propagation direction of the helical axis perpendicular to the film plane, which is simpler than that in MnGe. As reported in the literature, FeGe and MnSi films exhibit an additional magnetic phase transition when the magnetic field is applied perpendicular to the film plane, which is similar to the behavior observed in MnGe films. Through experimental analysis, the changes in the magnetic structure of FeGe and MnSi films under different magnetic field orientations have been attributed to the influence of uniaxial magnetic anisotropy. Specifically, when the magnetic field is applied parallel to the plane (i.e., perpendicular to the propagation direction of the helical axis), the direction of the helical axis remains unchanged, while the helical period changes, transitioning from three turns to two turns through an incommensurate state.[30] When the magnetic field is applied perpendicular to the film plane (i.e., parallel to the propagation direction of the helical axis), the helical magnetic state transitions into a conical state without an additional magnetic phase transition. This physical model clearly explains the unusual magnetoresistance and M–H behavior observed in FeGe and MnSi films, but it may not fully account for the magnetic anisotropy observed in MnGe thin films, as MnGe possesses a more complex magnetic structure compared to other B20 materials.

As mentioned above, MnGe films host a complex multi-domain ground state with tilted helical axes,[10,14] leading to the observed metamagnetic transition, robust low-field positive magnetoresistance, and Seebeck plateau under in-plane fields — features absent in simpler helical systems. This enhanced complexity stems from MnGe's intrinsic triple-q magnetic instability, which drives the reorientation of helical axes toward the [111] direction in thin films.[10] The pronounced positive magnetoresistance in MnGe, peaking near phase boundaries, differs fundamentally from the monotonic negative magnetoresistance in FeGe/MnSi, suggesting a distinct scattering mechanism potentially linked to emergent field fluctuations or multi-to-single domain transitions rather than conventional spin-disorder suppression.[17] Furthermore, the stability of the Seebeck plateau at low in-plane fields in MnGe implies a magnetic rigidity not observed in other B20 films, underscoring the unique energetics of its multi-domain configuration. These comparative differences highlight how MnGe's intricate magnetic texture manifests in transport and thermodynamic properties distinct from its B20 counterparts.

Through measurements of magnetoresistance, M–H curves, the magneto-Seebeck effect, and MFM, we found that MnGe thin films exhibit both in-plane and out-of-plane magnetic anisotropy. Notably, compared to H perpendicular to the (111) plane, nonlinear M–H curves and positive magnetoresistance at low magnetic fields appear in MnGe films when H is parallel to the (111) plane. MFM images further reveal that the magnetic structure of MnGe thin films remains unchanged at low magnetic fields below the magnetic transition temperature, and by combining all transport measurements with H parallel to the (111) plane, we constructed a phase diagram, which aligns with the behavior observed in the MFM data.

These results significantly contribute to a better understanding of the magnetic interactions in MnGe thin films. Additionally, we provide a comprehensive set of methods for studying materials with complex magnetic structures, which may prove beneficial for future studies of other materials with similarly complex magnetic properties.

Acknowledgments

This work was supported by the National Natural Science Foundation of China (Grant Nos. 12488201, 12274390, 12304035, and 51627901), the Anhui Initiative in Quantum Information Technologies (Grant No. AHY160000), the Innovation Program for Quantum Science and Technology (Grant No. 2021ZD0302802), the National Key R&D Program of the MOST of China (Grant No. 2022YFA1602600), the Basic Research Program of the Chinese Academy of Sciences Based on Major Scientific Infrastructures (Grant No. JZHKYPT-2021-08), and the National Key R&D Program of China (Grant No. 2023YFA1607701). We thank the staff members of the SMA System (https://cstr.cn/31125.02.SHMFF.SM2.SMA) at the Steady High Magnetic Field Facility, CAS (https://cstr.cn/31125.02.SHMFF), for providing technical support and assistance in data collection and analysis.

References

[1] Mühlbauer S, Binz B, Jonietz F, Pfleiderer C, Rosch A, Neubauer A, Georgii R and Böni P 2009 *Science* **323** 915
[2] Yu X Z, Onose Y, Kanazawa N, Park J H, Han J H, Matsui Y, Nagaosa N and Tokura Y 2010 *Nature* **465** 901
[3] Li Y F, Kanazawa N, Yu X Z, Tsukazaki A, Kawasaki M, Ichikawa M, Jin X F, Kagawa F and Tokura Y 2013 *Phys. Rev. Lett.* **110** 117202
[4] Huang S X and Chien C L 2012 *Phys. Rev. Lett.* **108** 267201
[5] Gayles J, Freimuth F, Schena T, Lani G, Mavropoulos P, Duine R A, Blugel S, Sinova J and Mokrousov Y 2015 *Phys. Rev. Lett.* **115** 036602
[6] Shanavas K V and Satpathy S 2016 *Phys. Rev. B* **93** 195101
[7] Dhital C, DeBeer-Schmitt L, Zhang Q, Xie W, Young D P and DiTusa J F 2017 *Phys. Rev. B* **96** 214425
[8] Turgut E, Paik H J, Nguyen K, David A M, Darrell G S and Gregory D F 2018 *Phys. Rev. Mater.* **2** 074404
[9] Tanigaki T, Shibata K, Kanazawa N, Yu X Z, Onose Y, Park H S, Shindo D and Tokura Y 2015 *Nano Lett.* **15** 5438
[10] Kanazawa N, White J S, Rnnow H M, Dewhurst C D, Morikawa D, Shibata K, Arima T, Kagawa F, Tsukazaki A, Kozuka Y, Ichikawa M, Kawasaki M and Tokura Y 2017 *Phys. Rev. B* **96** 220414
[11] Fujishiro Y, Kanazawa N, Kurihara R, Ishizuka H, Hori T, Yasin F S, Yu X, Tsukazaki A, Ichikawa M, Kawasaki M, Nagaosa N, Tokunaga M and Tokura Y 2021 *Nat. Commun.* **12** 317
[12] Kanazawa N, Kitaori A, White J S, Ukleev V, Rnnow H M, Tsukazaki A, Ichikawa M, Kawasaki M and Tokura Y 2020 *Phys. Rev. Lett.* **125** 137202
[13] Hayashi Y, Okamura Y, Kanazawa N, Yu T, Koretsune T, Arita R, Tsukazaki A, Ichikawa M, Kawasaki M, Tokura Y and Takahashi Y 2021 *Nat. Commun.* **12** 5974
[14] Repicky J, Wu P K, Liu T, Corbett J P, Zhu T, Cheng S, Ahmed A S, Takeuchi N, Guerrero-Sanchez J, Randeria M, Kawakami R K and Gupta J A 2021 *Science* **374** 1484
[15] Pomjakushin V, Plokhikh I, White J S, Fujishiro Y, Kanazawa N, Tokura Y and Pomjakushina E 2023 *Phys. Rev. B* **107** 024410
[16] Engelke J, Menzel D and Dyadkin V A 2013 *J. Phys.: Condens. Matter* **25** 472201
[17] Kanazawa N, Nii Y, Zhang X X, Mishchenko A S, De Filippis G, Kagawa F, Iwasa Y, Nagaosa N and Tokura Y 2016 *Nat. Commun.* **7** 11622
[18] Fujishiro Y, Kanazawa N, Shimojima T, *et al.* 2018 *Nat. Commun.* **9** 408
[19] Pollard S D, Garlow J A, Yu J W, Wang Z, Zhu Y M and Yang H 2017 *Nat. Commun.* **8** 14761
[20] Jiang W J, Zhang S, Wang X, Phatak C, Wang Q, Zhang W, Jungfleisch M B, Pearson J E, Liu Y Z, Zang J D, Cheng X M, Petford-Long A, Hoffmann A and te Velthuis S G E 2019 *Phys. Rev. B* **99** 104402
[21] Wortmann D, Heinze S, Kurz P, Bihlmayer G and Blugel S 2001 *Phys. Rev. Lett.* **86** 4132
[22] Schlickum U, Wulfhekel W and Kirschner J 2003 *Appl. Phys. Lett.* **83** 2016
[23] Milde P, Khler L, Neuber E, Ritzinger P, Garst M, Bauer A, Pfleiderer C, Berger H and Eng L M 2020 *Phys. Rev. B* **102** 024426
[24] Li H, Qi X Y, Wu J, Zeng Z Y, Wei J and Zhang H 2013 *ACS Nano* **7** 2842
[25] Xiang K, Hou Y B, Wang J H, Zhang J, Feng Q Y, Wang Z, Meng W J, Lu Q Y and Lu Y L 2022 *Rev. Sci. Instrum.* **93** 093706
[26] Guo T F, Wang J H, Meng W J, Zhang J, Feng Q Y, Wang Z, Jin F, Wu W B, Lu Q Y, Hou Y B and Lu Q Y 2020 *Ultramicroscopy* **217** 113071
[27] Schoenherr P, Mller J, Khler L, Rosch A, Kanazawa N, Tokura Y, Garst M and Meier D 2018 *Nat. Phys.* **14** 465
[28] Schoenherr P, Stepanova M, Lysne E N, Kanazawa N, Tokura Y, Bergman A and Meier D 2021 *ACS Nano* **15** 17508
[29] Dussaux A, Schoenherr P, Koumpouras K, Chico J, Chang K, Lorenzelli L, Kanazawa N, Tokura Y, Garst M, Bergman A, Degen C L and Meier D 2016 *Nat. Commun.* **7** 12430
[30] Kanazawa N, White J S, Rnnow H M, Dewhurst C D, Fujishiro Y, Tsukazaki A, Kozuka Y, Kawasaki M, Ichikawa M, Kagawa F and Tokura Y 2016 *Phys. Rev. B* **94** 184432
[31] Yokouchi T, Kanazawa N, Tsukazaki A, Kozuka Y, Kikkawa A, Taguchi Y, Kawasaki M, Ichikawa M, Kagawa F and Tokura Y 2015 *J. Phys. Soc. Jpn.* **84** 104708